Restoration of pharyngeal dilator muscle force in dystrophin deficient (*mdx*) mice following co-treatment with neutralising IL-6 receptor antibodies and Urocortin-2

David P. Burns[1], Jane Rowland[2], Leonie Canavan[2], Kevin H. Murphy[1], Molly Brannock[2], Dervla O'Malley[1], Ken D. O'Halloran[1] and Deirdre Edge[2]

[1]Department of Physiology, School of Medicine, University College Cork, Cork, Ireland

[2]Department of Physiology, Trinity Biomedical Sciences Institute, Trinity College Dublin, the University of Dublin, Dublin, Ireland

Corresponding author

Dr. Deirdre Edge

Department of Physiology,

Trinity Biomedical Sciences Institute,

Trinity College Dublin,

Dublin 2,

Ireland.

Tel: +353 1 896 2710

Email: edged@tcd.ie

Short title: Immune and stress factors contribute to pharyngeal dilator weakness in *mdx* mice

Subject area: Muscle Physiology

Three key words: Duchenne muscular dystrophy, respiratory muscle, interleukin-6

This is an Accepted Article that has been peer-reviewed and approved for publication in the Experimental Physiology, but has yet to undergo copy-editing and proof correction. Please cite this article as an Accepted Article; doi: 10.1113/EP086232.

Total number of words: 9321

Total number of references: 63

Abbreviations: SDB, sleep disordered breathing; CRF, corticotrophin releasing factor; CRFR, CRF receptor; TNF, tumor necrosis factor; IL, interleukin; IL-6R, interleukin-6 receptor; Uro-2, urocortin2; MHC, myosin heavy chain; WT, wild-type; xIL-6R, anti-IL-6R; CSA, cross-sectional area; L_o, optimum length; CT, contraction time; ½ RT, half relaxation time; Smax, total shortening; Vmax, shortening velocity.

What is the central question of this study?

Duchenne muscular dystrophy (DMD) is associated with severe muscle weakness, with inflammation recognised as a contributing factor to DMD pathology. We have previously reported impaired upper airway dilator muscle function in the *mdx* mouse model of DMD. Our aim was to assess the effect of blocking interleukin-6 receptor signalling and stimulating corticotrophin releasing factor receptor 2 signalling on *mdx* sternohyoid muscle structure and function.

What is the main finding and its importance?

The combined anti-inflammatory and anti-stress interventional treatment had a positive inotropic effect on sternohyoid muscle force, restoring mechanical work and power to wild type values. Furthermore, drug treatment reduced myofibre central nucleation and preserved the MHC type IIb fibre complement of *mdx* sternohyoid muscle. These data may have implications for the development of pharmacotherapies for DMD with relevance to respiratory muscle performance.

Abstract

The *mdx* mouse model of Duchenne muscular dystrophy (DMD) shows evidence of impaired pharyngeal dilator muscle function. We hypothesised that inflammatory and stress-related factors are implicated in airway dilator muscle dysfunction. Six week old *mdx* (n=26) and wild-type (WT; n=26) mice received either saline (0.9% w/v) or a co-administration of neutralising IL-6 receptor antibodies (xIL-6R; 0.2 mg/kg) and corticotrophin releasing factor receptor 2 agonist (Urocortin 2; 30μg/kg) over 2 weeks. Sternohyoid muscle isometric and isotonic contractile function was examined *ex vivo*. Muscle fibre centronucleation, and muscle cellular infiltration, collagen content, fibre type distribution and fibre cross-sectional area were determined by histology and immunofluorescence. Muscle chemokine content was examined by use of a multiplex assay. Sternohyoid peak specific force at 100Hz was significantly reduced in *mdx* compared with WT. Drug treatment completely restored force in *mdx* sternohyoid to WT levels. The percentage of centrally-nucleated muscle fibres was significantly increased in *mdx* and this was partially ameliorated following drug treatment. The areal density of infiltrates and collagen content were significantly increased in *mdx* sternohyoid; both indices were unaffected by drug treatment. The abundance of MHC type IIb fibres was significantly decreased in *mdx* sternohyoid; drug treatment preserved MHC type IIb complement in *mdx* muscle. The chemokines MIP-2, IP-10 and MIP-3α were significantly increased in *mdx* sternohyoid compared with WT. Drug treatment significantly increased chemokine expression in *mdx* but not WT. Recovery of contractile function was impressive in our study with implications for DMD. The precise molecular mechanisms by which the drug treatment exerts an inotropic effect on *mdx* sternohyoid muscle remains to be elucidated.

Keywords

DMD, *mdx*, interleukin-6, stress, corticotrophin releasing factor, sternohyoid muscle.

1. Introduction

Duchenne muscular dystrophy (DMD) is a fatal neuromuscular disease that occurs in 1:3,500 male births (Emery, 1991). Patients have defects in the dystrophin gene, which results in a lack of the structural protein dystrophin (427 kDa). Dystrophin is a rod-shaped protein expressed in skeletal, cardiac and smooth muscle, where it links cytoskeleton actin to the sarcolemma and has a physiological role in preventing damage during muscle contraction (Nowak & Davies, 2004). The absence of dystrophin in DMD induces severe damage to muscle fibres, with resultant inflammation (Deconinck & Dan, 2007). As the disease progresses there is a loss of functional muscle fibres due to necrosis and the deposition of fibrotic and adipose tissue prevails, resulting in muscle weakness.

The respiratory system is severely impaired in DMD due to respiratory and abdominal muscle weakness, as well as scoliosis (De Bruin *et al.*, 1997; Beck *et al.*, 2006). DMD is a progressive disease and thus respiratory function deteriorates with age, with patients often presenting with reduced vital capacity and breathing disturbances such as hypoventilation and sleep-disordered breathing (SDB) (Smith *et al.*, 1989; Hill *et al.*, 1992; Barbé *et al.*, 1994). While the diaphragm has been the focus of many studies in this field, there is a paucity of information pertaining to the upper airway muscles controlling airway calibre and collapsibility, thereby facilitating breathing (White & Younes, 2012). The prevalence of obstructive sleep apnoea (OSA) in DMD (Suresh *et al.*, 2005), suggests that upper airway muscle dysfunction, and poor control of airway patency during sleep, potentially contributes to breathing disturbances in DMD.

The *mdx* mouse is the most widely studied animal model of DMD. We have previously reported respiratory dysfunction, which presents at an early age in the *mdx* mouse (8 weeks), consisting of hypoventilation and upper airway (sternohyoid) muscle weakness (Burns *et al.*, 2015; Burns & O'Halloran, 2016). In human patients and *mdx* mice, functional impairments are driven by pathological changes in skeletal muscles due to dystrophin deficiency, including fibre degeneration

and necrosis, with inflammation thought to play an integral part in DMD muscle pathology (Deconinck & Dan, 2007).

In patients and *mdx* mice, sarcolemmal damage is accompanied by the infiltration of immune cells, primarily macrophages and T cells, a key source of inflammatory cytokines (Moran & Mastaglia, 2014). These molecules mount an inflammatory response through activation of additional cytokines and recruitment of further immune cells to the damaged muscle (Villalta *et al.*, 2015). Immune cells are not the only source of cytokines, with damaged muscles fibres also serving as a contributory factor (Whitham & Febbraio, 2016). In DMD, the heightened expression of pro-inflammatory cytokines such as tumour necrosis factor alpha (TNF-α) and interleukins (IL)-1 and -6, are early disease indicators and are associated with exacerbation of the inflammatory response in dystrophic muscle (Evans *et al.*, 2009b, a). IL-6 is released from a variety of tissues including immune cells and adipocytes and is commonly referred to as a myokine as it can be secreted from muscle in response to physical activity (Jonsdottir *et al.*, 2000; Pedersen & Febbraio, 2008). This inflammatory cytokine is of particular interest in DMD pathology since it is elevated in muscle and plasma samples from DMD patients (Messina *et al.*, 2011; Rufo *et al.*, 2011; Pelosi *et al.*, 2015a) and *mdx* mice (Pelosi *et al.*, 2015a). IL-6 is pleiotropic, however it mediates its pro-inflammatory effects via its trans-signalling pathway by use of the soluble IL-6 receptor (IL-6R) (Pedersen & Febbraio, 2008). Its importance in *mdx* skeletal muscle pathology was recently highlighted (Pelosi *et al.*, 2015a), showing that blockade of IL-6 signalling in *mdx* mice has beneficial functional outcomes in dystrophic skeletal muscle.

Muscle wasting is a common feature of DMD due to muscle proteolysis, thus pharmacological interventions aimed at rescuing muscle are attractive. Corticotrophin releasing factor receptor 2 (CRFR2) agonists have been shown to modulate muscle mass through the activation of anabolic signalling pathways and a capacity to alter the rate of proteolysis during atrophying conditions (Hall *et al.*, 2007). In addition, CRFR2 can reduce nerve damage, corticosteroid-induced atrophy and loss of muscle mass due to immobilisation (Hinkle *et al.*, 2003). The CRFR2 agonist, Urocortin 2 (Uro-2), has been shown to improve diaphragm function and reduce fibrosis and immune cell infiltration in

mdx mice (Reutenauer-Patte *et al.*, 2012). Recent work demonstrated that neutralisation of IL-6 receptor (xIL-6R) or stimulation of CRFR2 both had positive inotropic effects on the major pump muscle of breathing – the diaphragm (Manning *et al.*, 2017). Furthermore, Manning et al. (2017) reported that co-treatment of xIL-6R and Uro-2 had an additive inotropic effect on diaphragm muscle force. We hypothesised that co-administration of xIL-6R antibodies and Uro-2 alleviates upper airway muscle weakness in dystrophin deficient *mdx* mice. We sought to examine structure and function of sternohyoid muscle (pharyngeal dilator) from age-matched wild type (WT) and *mdx* mice following saline or combined xIL-6R and Uro-2 drug treatment.

2. Methods

2.1 Ethical approval

All procedures were performed under licence in accordance with National and European guidelines following local research ethics committee approval.

2.2 Animals

Male and female wild type (WT; C57BL/10ScSnJ) and *mdx* (C57BL/10ScSn-Dmd^{mdx}/J) mice were purchased from the Jackson Laboratory (Jackson Laboratory, Bar Harbor, ME) and were bred in our institution's animal housing facility. Animals were housed conventionally in a temperature- and humidity-controlled facility, operating on a 12 h light: 12 h dark cycle with food and water available *ad libitum*. 6 week old male WT and *mdx* mice received a treatment consisting of a co-administration of xIL-6R (IL-6R neutralising antibody; MR1-61 (Okazaki *et al.*, 2002); 0.2 mg/kg) and Uro-2 (CRFR2 agonist; 30 µg/kg; U9507, Sigma Aldrich, Wicklow, Ireland) or saline (vehicle control; 0.9% w/v). MR1-61 stock was kept at -80^{o}C and Uro-2 stock at -20^{o}C. A working solution containing both MR1-61 (26.7µg/ml) and Uro-2 (4µg/ml) was made in sterile saline, aliquoted and stored at -20^{o}C until day of injection. Doses and treatment protocol were chosen based on previous studies (Manning *et al.*, 2016, 2017). Treatment consisted of six sub-cutaneous injections to the scruff of the neck on

alternate days over the course of two weeks beginning at 6 weeks of age. A 20g mouse received an injection bolus of 150µl. WT and *mdx* animals were assigned at random to saline or drug treatment, establishing 4 groups: WT saline (21.4 ± 1.6g; n=13), WT treatment (22.0 ± 1.2g; n=13), *mdx* saline (24.4 ± 1.6g; n=13) and *mdx* treatment (24.5 ± 1.7g; n=13). Animals were anaesthetised with 5% isoflurane by inhalation in oxygen and euthanised by cervical dislocation.

2.3 Muscle physiology

2.3.1 Ex vivo muscle preparation

The sternohyoid muscles were immediately excised and placed in a tissue bath at room temperature containing continuously gassed hyperoxic (95% O_2/ 5% CO_2) Krebs solution (NaCl 120 mM, KCl 5mM, Ca^{2+} gluconate 2.5 mM, $MgSO_4$ 1.2 mM, NaH_2PO_4 1.2 mM, $NaHCO_3$ 25mM, glucose11.5mM) and D-tubocurarine (25µM). The paired sternohyoid muscles were carefully separated along a natural division in the midline. One half was used immediately for functional analysis and the other half was snap frozen in liquid nitrogen for subsequent molecular analysis (section 2.5). A single longitudinal muscle strip (2mm in diameter) for each animal was studied in a water-jacketed muscle bath, containing Krebs solution, maintained at 35^{o}C gassed with 95% O_2/ 5% CO_2. Each muscle strip was placed between a pair of platinum plate electrodes, with the caudal end fixed to an immobile hook and the rostral end attached to a dual-mode lever transducer system by non-elastic string. Muscle preparations were allowed a 5 min equilibration period.

2.3.2 Isometric protocol

Following equilibration, the optimum length (L_o) was determined by adjusting the position of the force transducer by use of a micro-positioner between intermittent twitch contractions. The L_o was taken as the muscle length associated with maximal isometric twitch force in response to single isometric twitch stimulation (supramaximal stimulation, 1ms duration). Once L_o was determined, the muscle stayed at this length for the duration of the protocol. A single isometric twitch was measured.

Peak isometric twitch force, contraction time (CT; time to peak force) and half relaxation time (½ RT; time for peak force to decay by 50%) were determined. Next, an isometric tetanic contraction was elicited by stimulating muscle strips with supramaximal voltage at 100 Hz for 300 ms duration. Peak isometric tetanic force was determined at 100Hz (O'Halloran, 2006; Burns & O'Halloran, 2016).

2.3.3 Isotonic protocol

Following the isometric protocol, concentric contractions were elicited in incremental steps with varying load (0%, 5%, 10%, 15%, 20%, 25%, 30%, 35%, 40%, 60%; % of force at 100Hz) with 30 s rest between each contraction. Muscle length returned to L_o following each contraction. Total shortening was determined as the maximum distance shortened during contraction. Shortening velocity was determined as the distance shortened during the initial 30 ms of shortening (Lewis *et al.*, 2015; Lewis *et al.*, 2016). Mechanical work (force x total shortening) and power (force x shortening velocity) were determined at each step of the incremental load step test (Lewis *et al.*, 2015; Williams *et al.*, 2015; Burns & O'Halloran, 2016; O'Leary & O'Halloran, 2016).

2.4 Muscle immunohistochemistry and histology

2.4.1 Tissue preparation

The sternohyoid muscles were excised and divided down the midline; one half was embedded in optimum cutting temperature (OCT) embedding medium and frozen in isopentane cooled in liquid nitrogen and stored at -80^{o}C for subsequent structural analysis (n=4-5 per group). The other half of the muscle was placed in 4% paraformaldehyde overnight at 4^{o}C before being transferred to 70% ethanol prior to tissue processing and paraffin embedding for histological analysis (n=4-5 per group).

2.4.2 Myosin heavy chain fluorescence immunohistochemistry

Serial transverse muscle sections (10 μm) were cryo-sectioned (Model CM30505; Leica Microsystems, Nussloch, Germany) at –22^{o}C and mounted on polylysine-coated glass slides (VWR

International, Dublin, Ireland). Sections were captured from the middle belly and distal regions of the muscle. Slides were immersed in PBS (0.01 M) containing 1% bovine serum albumin (BSA) for 15 minutes. After 3x5 minute PBS washes, slides were immersed in PBS containing 5% goat serum for 30 minutes. Following a further 3x5 minute PBS rinses, slides were incubated with an unconjugated AffiniPure Fab Fragment Goat Anti-Mouse IgG (H+L) diluted in PBS (1:13, Jackson ImmunoResearch Labs) for 1 hour at room temperature, to enable the use of mouse monoclonal primary antibody staining on mouse tissue. After 3x2 minute washes in PBS, primary antibodies were applied. Primary monoclonal myosin antibodies were obtained from the Developmental Studies Hybridoma Bank (DSHB), University of Iowa, Iowa City, IA, USA and a rabbit anti-laminin antibody was obtained from Sigma-Aldrich (L9393). A triple-labelling approach was applied to tag MHC types I (BAD5, 1:100), IIa (sc71 1:100) and IIb (BFF3 1:100) on a single section. On a serial section, a double-labelling approach consisted of a rabbit anti-laminin antibody (1:500) and a pan-MHC antibody for the indirect determination of pure MHC IIx fibres, BF35 (1:50), labelling all MHC isoforms but IIx, enabling visualisation of IIx fibres by absence of staining; all antibodies were diluted in PBS and 1% BSA solution. Triple and double labelling solutions were applied on alternate sections on each slide. Individual sections were encircled with a hydrophobic pen (ImmEdgeTM Vector Labs) to prevent contamination from neighbouring sections on the same slide. Slides were incubated with the primary antibodies overnight at 4^{o}C in a humidity chamber.

After the incubation period, slides were washed with PBS for 3x5 minutes before the appropriate secondary antibodies were applied. All secondary antibodies were diluted in PBS and 1% BSA. For the triple-labelled slides, a cocktail of secondary antibodies was prepared containing AlexaFluor350-conjugated goat anti-mouse IgG2b (1:500, Invitrogen, Biosciences Ltd, Dun Laoghaire, Ireland), Dylight594-conjugated goat anti-mouse IgG1 (1:500, Jackson ImmunoResearch Europe Ltd, Suffolk, UK) and AlexaFluor488-conjugated goat anti-mouse IgM (1:250, Invitrogen), targeting MHC I, IIa and IIb, respectively. Secondary antibodies for double-labelled sections were Dylight594-conjugated goat anti-mouse IgG1 (1:500, Jackson) and FITC-conjugated anti-rabbit secondary antibody (1:250,

Sigma-Aldrich). Secondary antibodies were applied and slides were incubated for 1 hour in the dark at room temperature. Slides were rinsed with PBS for 3x5 minutes, cover slipped with polyvinyl alcohol mounting medium with DABCO® anti-fade (Sigma) before observation with a fluorescent microscope (Olympus BX51). Negative controls were also performed in which primary antibodies were omitted and sections were instead incubated in diluent. Images were merged using ImageJ software (W. S. Rasband, ImageJ; US National Institutes of Health, Bethesda, MD, USA).

2.4.3 Histological Analysis

Muscle samples were dehydrated (70% ethanol, 80% ethanol, 95% ethanol, 60 minutes each) and then placed in 100% ethanol (60 minutes x2). Samples were then cleared in xylene (60 minutes x2), before being transferred to two changes of paraffin (one hour each) (Leica TP1020, Histokinet). Tissue samples were then embedded in paraffin (Sakura Tissue-Tek TEC, Histolab Histowax embedding medium), and serial cross-sections (5 μm thick) were sectioned using a microtome (Leica RM2135). Serial sections were collected throughout the muscle (mid-belly and distal regions) onto glass slides and oven-dried (overnight at 37°C).

To examine putative inflammatory cell infiltration, and central nucleation of muscle fibres, tissue sections were stained with haematoxylin and eosin (H&E). Tissue sections were deparaffinised in xylene (2 x 5 minutes each), rehydrated through a graded series of alcohols (100% ethanol, 95% ethanol, 70% ethanol, one minute each). Sections were stained with haematoxylin (Delafield's Haematoxylin) (5 min) and subsequently rinsed in distilled H_2O (5 min), stained in eosin (alcoholic Eosin-Y, Sigma Aldrich; 1 min), rinsed in distilled H_2O, and dehydrated (70% ethanol, 95% ethanol, 1 min each, 100% ethanol, 2 x 1 minute) and xylene (5 min). For collagen staining, a Masson's trichrome protocol was followed (Sigma Aldrich). Slides were mounted using DPX mounting medium (Sigma Aldrich, USA), air-dried and visualised on a bright field microscope (Olympus BX51) x 20 magnification.

2.5 Molecular studies

2.5.1 Tissue preparation

Sternohyoid samples stored at -80°C were removed and allowed to defrost at 4°C for 5 minutes. All procedures were performed at 4°C to prevent protein degradation. Samples were homogenized in a lysis buffer (RIPA) made up from 10X RIPA, deionized water, 200mM sodium fluoride (NAF), 100mM phenylmethylsulfonylfluoride (PMSF), protease cocktail inhibitor 1 and phosphatase cocktail inhibitor 2. Following the homogenization process, the reactant mixtures were centrifuged (14,000 x rpm) at 4°C for 20 min and the supernatants were harvested. Total amount of protein for each tissue sample was determined using Pierce ® Bicinchoninic Acid Assay (BCA assay, Thermo Scientific, Fisher, Dublin, Ireland). Supernatants were stored at -80°C for future use.

2.5.2 Chemokines

A chemokine assay (U-PLEX Chemokine Combo; K15099K-1, Meso Scale Discovery, Rockville, MD) was used to examine chemokines in sternohyoid muscle from all four groups: WT saline (n=7-8), WT treatment (n=7-8), *mdx* saline (n=8) and *mdx* treatment (n=7). The assay was performed according to the manufacturer's instructions using an extended incubation time to improve detection (the plate was incubated overnight at 4°C). Following incubation, the plate was read on QuickPlex SQ 120 imager (Meso Scale Discovery, Rockville, MD). Signals within the detectable range were achieved with reliability for the following 3 chemokines: macrophage inflammatory protein 2 (MIP-2), interferon-γ-induced protein 10 (IP-10) and macrophage inflammatory protein-3α (MIP-3α).

2.6 Data and image analysis

Specific force was calculated in N/cm^2 of estimated muscle cross-sectional area (CSA). The CSA of each strip was determined by dividing the muscle mass (weight in grams) by the product of muscle L_o (cm) and muscle density (assumed to be 1.06 g/cm^3). The CT and ½ RT were measured as indices of isometric twitch kinetics. For isotonic load relationships, data were plotted as the measured variable versus % load. Total muscle shortening was normalised to L_o and expressed in L/L_o. Similarly,

shortening velocity was normalised to L_o and expressed in L_o/s. Maximum total shortening (Smax) and maximum shortening velocity (Vmax) were measured when both were maximal at 0% load. Mechanical work was measured in J/cm^2. Mechanical power was expressed in W/cm^2. Maximum mechanical work (Wmax) and power (Pmax) were also measured and typically occurred between 30% and 40% load.

For MHC fibre type analysis, muscle sections were viewed at x10 magnification and images captured using an Olympus BX51 microscope and an Olympus DP71 camera. Cell Sens™ (Olympus) was used to digitally capture the images. Analysis was carried out using image J software, where fibre type CSA and fibre type distribution for each MHC fibre type were determined. CSA measurements were made by fibre "circling" based on MHC labelling. A square test frame (640,000 μm^2) with inclusion and exclusion boundaries was employed to calculate these parameters in a given randomly chosen field. For each animal, multiple sections throughout the length of the muscle were viewed and 3-4 images analysed per fibre type. H&E stained sections were visualised x20 magnification. Six sections were examined across the muscle from the rostral, middle and caudal regions. Two randomly selected areas were captured per muscle section from non-overlapping areas for analysis. Muscle pathology was scored using ImageJ software. The number of myofibres displaying central nucleation was expressed as a percentage of the total number of myofibres per image. Putative inflammatory cell infiltration (the presence of cells in the extracellular matrix), was also scored and expressed as a percentage of the total area of muscle. For Masson's trichrome staining, the microscope lighting exposure was maintained throughout. Three sections, with two images captured per section, from the mid-portion of the muscle, were analysed per animal. Images were analysed using a colour balance threshold (ImageJ software), and the area of collagen was expressed as a percentage of the total area of muscle. For chemokine analysis, chemokine signals within the detectable range were expressed as relative fluorescence units per μg protein (RFU/μg protein), with equal protein loading in all wells.

2.7 Statistical Analysis

Values are expressed as mean ± S.D. Muscle functional data were statistically compared using two-way ANOVA (genotype x treatment) with Bonferroni post-hoc test. For muscle histology, group means were generated from multiple images averaged per animal and then compared by two-way ANOVA (genotype x treatment) with Bonferroni post-hoc test. $P < 0.05$ was deemed to be statistically significant.

3. Results

3.1 Body mass

There was a significant difference in body mass ($p < 0.0001$; two-way ANOVA) between age-matched WT and *mdx* mice; the latter were slightly heavier. Drug treatment had no effect on body mass.

3.2 Isometric force and twitch contractile kinetics

Table 1 shows data for sternohyoid muscle twitch force and contractile kinetics (CT and ½ RT) from animals following drug or saline treatment. *Mdx* sternohyoid twitch force was significantly lower ($p = 0.01$ (genotype); two-way ANOVA) compared with WT. Post hoc analysis revealed that drug treatment significantly increased twitch force in *mdx* sternohyoid ($p < 0.01$; two-way ANOVA with Bonferroni), but not in WT ($p > 0.05$). There was no significant difference between WT and *mdx* in values for CT and ½ RT; both were unaffected by drug treatment. Although statistical differences were not observed for CT and ½ RT across groups, sizeable effects were noticed which could have physiological relevance. CT was increased by ~45% and ½ RT by ~28% for *mdx* sternohyoid compared with WT. Treatment reduced CT by ~18% and ½ RT by ~19% in *mdx* mice. Peak force at 100Hz was significantly lower in *mdx* sternohyoid ($p = 0.0003$) compared with WT (Fig. 1). Post hoc analysis showed

that drug treatment significantly increased force for WT ($p < 0.01$) and *mdx* ($p < 0.01$) sternohyoid.

3.3 Isotonic contractile parameters and kinetics

Table 1 shows data for sternohyoid muscle isotonic contractile parameters: Wmax, Pmax, Smax and Vmax. Wmax was significantly reduced in *mdx* sternohyoid ($p = 0.004$; two-way ANOVA) compared with WT. Drug treatment significantly increased Wmax for WT ($p < 0.05$; two-way ANOVA with Bonferroni), but not *mdx* muscle ($p > 0.05$). Pmax was significantly reduced in *mdx* sternohyoid ($p = 0.0003$) compared with WT, and drug treatment significantly increased Pmax in *mdx* ($p = 0.01$). Vmax was significantly reduced in *mdx* sternohyoid ($p = 0.008$) compared with WT, and this was unaffected by drug treatment. There was no significant difference in Smax between WT and *mdx*. Drug treatment had no effect on Smax in both groups.

3.4 Isotonic load relationships

Fig. 2 (A-D) shows data for sternohyoid muscle isotonic load relationships. Loading had a significant effect on work ($p < 0.0001$; two-way ANOVA; Fig. 2A), power ($p < 0.0001$; Fig. 2B), shortening ($p < 0.0001$; Fig. 2C) and shortening velocity ($p < 0.0001$; Fig. 2D) for both WT and *mdx* sternohyoid. *Mdx* muscle had significantly reduced work ($p < 0.0001$), power ($p < 0.0001$) and shortening velocity ($p < 0.0001$) compared with WT. Drug treatment significantly increased work production for WT ($p < 0.0001$; two-way ANOVA with Bonferroni) and *mdx* muscle ($p < 0.0001$). Power production was also significantly increased for WT ($p < 0.0001$) and *mdx* ($p < 0.0001$) sternohyoid following drug treatment. Shortening velocity was significantly increased for *mdx* muscle ($p = 0.02$) following drug treatment.

3.5 MHC fibre type distribution

Type I fibres were absent from sternohyoid muscle in all groups. A positive control image for type I fibre staining in WT mouse diaphragm muscle is shown in Fig. 3A. The fibre type distribution of type IIa fibres did not vary significantly between the four groups (Fig. 3B). For *mdx* saline, the distribution of type IIx fibres was significantly increased compared with WT saline (Fig. 3C; $p < 0.0001$; two-way ANOVA), whereas the distribution of type IIb fibres was significantly reduced in *mdx* saline compared with WT saline (Fig. 3D; $p < 0.01$). Sternohyoid fibre type changes were prevented/reversed by drug treatment in *mdx* with significant changes in type IIx (Fig. 3C; $p < 0.01$; two-way ANOVA with Bonferrroni) and type IIb fibres (Fig. 3D; $p < 0.05$) compared with *mdx* saline.

3.6 Fibre cross-sectional area

Figure 3E shows data for the CSA for all fibre types. There was a significant increase in the CSA of type IIa ($p < 0.05$; two-way ANOVA) and type IIx fibres ($p < 0.05$) in *mdx* sternohyoid compared with WT. Drug treatment had no significant effect on type IIa ($p = 0.08$) or type IIx ($p = 0.628$) CSA for both WT and *mdx*. The CSA of type IIb fibres were not significantly different between WT and *mdx*. With treatment, type IIb CSA was significantly increased in WT only ($p < 0.05$; two-way ANOVA with Bonferroni).

3.7 Central nucleation and putative inflammatory cell infiltration

The percentage of sternohyoid muscle fibres with centrally located nuclei was significantly increased in *mdx* (Fig 4A-B; $p < 0.0001$; two-way ANOVA) compared with WT sternohyoid. Central nucleation was reduced slightly in *mdx* mice following drug treatment compared with *mdx* saline (Fig 4A-B; $p < 0.05$; two-way ANOVA with Bonferroni). The areal density of inflammatory cell infiltration was significantly increased in *mdx* sternohyoid muscle (Fig 4A+C; $p < 0.001$; two-way ANOVA) compared with WT. Drug treatment had no significant effect on the relative area of putative immune cell infiltration (Fig 4A+C).

3.8 Collagen content

Masson's trichrome staining was applied to investigate muscle collagen content between groups. The percentage area of collagen was significantly increased in *mdx* sternohyoid compared with WT (Fig. 5A+B; $p = 0.0103$; two-way ANOVA). Drug treatment had no significant effect on collagen content for both WT ($p > 0.05$) and *mdx* ($p > 0.05$) sternohyoid.

3.9 Chemokines

Figure 6 shows data for chemokine content in sternohyoid muscle from WT and *mdx* mice following drug or saline treatment. MIP-2, IP-10 and MIP-3α were significantly increased in the *mdx* sternohyoid ($p < 0.0002$, MIP-2 and IP-10; $p = 0.004$, MIP-3α; two-way ANOVA) compared with WT controls. Post-hoc analysis revealed that drug treatment significantly increased MIP-2, IP-10 and MIP-3α in *mdx s*ternohyoid ($p < 0.0001$, MIP-2 and IP-10; $p < 0.01$ MIP-3α; two-way ANOVA with Bonferroni), but not in WT mice ($p > 0.05$, Fig. 6A-C).

4. Discussion

The key findings of the present study are: (1) Sternohyoid muscle weakness in *mdx* mice is evidenced by reduced specific force and power output; (2) Sternohyoid weakness is associated with changes in myosin heavy chain isoform expression, with an increase in the abundance of type IIx and a concomitant decrease in type IIb fibres; (3) The incidence of centrally-nucleated muscle fibres, percentage and areal density of inflammatory cell infiltrates, and deposition of collagen was significantly increased in *mdx* sternohyoid; (4) Chemokines were significantly increased in *mdx* sternohyoid; (5) Co-treatment with the xIL-6R antibody and Uro-2 restored mechanical force and power production in *mdx* sternohyoid muscle; (6) Drug treatment significantly prevented or reversed fibre transitions in *mdx* sternohyoid, reduced the proportion of centrally nucleated fibres, but did not affect the total area of putative inflammatory cell infiltration, or collagen content within *mdx* muscle; (7) Drug treatment significantly increased chemokines in *mdx* sternohyoid muscle.

Chronic respiratory insufficiency is a cardinal feature of DMD. The diaphragm is severely affected, with muscle fibre degeneration and fibrosis central characteristics of the disease (De Bruin et al., 1997). DMD patients often suffer from SDB, with episodes of hypoventilation during sleep, associated with aberrant blood gas disturbances, necessitating ventilator use at later stages to maintain respiratory function, (Hukins & Hillman, 2000).

The *mdx* mouse, a dystrophin deficient model (Bulfield *et al.*, 1984), has been studied extensively to understand the pathophysiology of DMD and has also served as a pre-clinical model for the study of pharmacological treatment strategies (Manning & O'Malley, 2015). As DMD progresses, cardiopulmonary failure is the leading cause of death (Hukins & Hillman, 2000). The dystrophin deficient *mdx* mouse has a milder phenotype than DMD patients in the

context of cardiac and limb muscle. In contrast, the respiratory muscles, including the sternohyoid muscle, show severe mechanical weakness at a young age in the *mdx* mouse (Burns & O'Halloran, 2016). Dystrophic diaphragm muscle undergoes repetitive cycles of degeneration and regeneration, with additional activation of inflammatory cascades that further exacerbate muscle weakness. Whilst diaphragm muscle function has been well characterised in DMD (De Bruin *et al.*, 1997), and the *mdx* mouse (Coirault *et al.*, 1999; Coirault *et al.*, 2003; Bates *et al.*, 2013), little is known about the complementary muscles of breathing, especially the airway dilator muscles of the pharynx that are critical in the control of airway calibre, which is surprising given the prevalence of SDB in DMD boys (Bersanini *et al.*, 2012).

In the present study, we demonstrate that *mdx* sternohyoid muscle shows impaired performance at 8 weeks of age, consistent with our recent report (Burns & O'Halloran, 2016). This functional impairment is characterised by reduced specific force (twitch and tetanic contractions), reduced maximum mechanical work and power production, and reduced Vmax. Work and power production as a function of load bearing was significantly reduced for *mdx* saline compared with WT saline. We observed a ~44% decrease in sternohyoid muscle peak tetanic force for *mdx* saline *versus* WT saline, which is consistent with previous findings (Attal *et al.*, 2000; Burns & O'Halloran, 2016). These studies reveal severe mechanical dysfunction in sternohyoid muscle from young and aged *mdx* mice suggesting that upper airway obstruction in DMD may be a result of increased collapsibility of the pharyngeal airway arising from dysfunction of upper airway dilator muscles.

Sternohyoid muscle weakness in *mdx* was associated with a shift in the myosin heavy chain isoform distribution. Contractile performance in muscle correlates with fibre type distribution

(Schiaffino & Reggiani, 2011). The sternohyoid muscle is phasically active during respiration (Van de Graaff *et al.*, 1984; O'Halloran *et al.*, 2002) and is composed solely of fast fibres (type II). Type II fibres display progressively increasing force production from type IIa to IIx fibres, with type IIb fibres producing the greatest forces but least resistance to fatigue (Polla *et al.*, 2004; Schiaffino & Reggiani, 2011). We observed a significant decrease in the relative proportion of type IIb fibres with a concomitant increase in the type IIx fibre count in *mdx* muscle. Since the type IIb fibres are the maximum force producing units with the fastest kinetics, this finding is consistent with the functional data demonstrating decreased force-generating capacity and reduced shortening velocity in *mdx* compared with WT. Our findings are consistent with the observations of others (Attal *et al.*, 2000), who likewise reported reduced force-generating capacity and an increased proportion of type IIx and reduced type IIb in sternohyoid muscle from aged (6 month) *mdx* mice. We reason that this shift in the fibre type composition of the sternohyoid relates to muscle fibre degeneration and regeneration such that the muscle is in a relatively immature state. Muscle fibre remodelling will also alter motor neuronal input to the muscle. Since muscle fibre types are determined by the motor unit they are innervated by (Mantilla & Sieck, 2003), it is plausible to speculate that dystrophic muscle may have an altered motor unit innervation pattern which warrants investigation. There is a paucity of information pertaining to the accessory muscles of breathing in *mdx* mice. Unlike the well-characterised *mdx* diaphragm, the temporal profile of *mdx* sternohyoid muscle structure-function relationship throughout life is unknown, but published works suggest that the sternohyoid most likely undergoes a similar pathology to *mdx* diaphragm muscle (Attal et al. 2000; Burns et al. 2016).

The CSA of a muscle fibre is a determinant of force production. CSA varies between fibres increasing from type I fibres to type IIa and IIx, and type IIb (figure 3E). In DMD, the cycles

of degeneration and regeneration within muscles leads to alterations in fibre size. As such, dystrophic muscle has myofibres of varying size compared to the uniformity of diameter found in a normal muscle (Pastoret & Sebille, 1995). Investigation of the CSA of individual muscle fibre types revealed that *mdx* sternohyoid shows evidence of hypertrophied type IIa and type IIx fibres. Increasing CSA can be viewed as an adaptive mechanism in the context of force production, often observed with resistance training increasing muscle strength. However, alterations in fibre size secondary to degeneration and regeneration are characteristic of *mdx* muscle with regeneration producing hypertrophied fibres, which are often functionally weaker (Lynch *et al.*, 2001).

Dystrophic skeletal muscle undergoes progressive cycles of fibre degeneration and regeneration following damage, a process that continues until the regenerative capacity is exhausted. Skeletal muscle fibre central nucleation is a histological indicator of muscle fibre repair and regeneration. We observed a significant increase in the percentage of centrally nucleated myofibres in *mdx* sternohyoid compared with WT, with ~25% of *mdx* sternohyoid fibres presenting with central nuclei. This reveals that sternohyoid muscle from *mdx* mice is undergoing significant muscle damage and repair as early as 8 weeks of age, consistent with evidence of severe muscle weakness.

Inflammation is recognised to be a contributing factor to DMD pathology, which is characterised by a persistent inflammatory response in skeletal muscle due to chronic damage and stress to functional muscle fibres due to the absence of dystrophin (Deconinck & Dan, 2007). Inflammatory cell infiltration of damaged and degenerating dystrophic muscle fibres is a hallmark feature of skeletal muscle pathology in DMD. Inflammatory cell infiltration has been shown to exacerbate myofibre damage in *mdx* mice (Evans *et al.*, 2009a), with loss of

muscle fibres, subsequent fibrosis, and adipose tissue deposition culminating in impaired muscle function (Deconinck & Dan, 2007). We observed a significant increase in putative inflammatory cell infiltration in young *mdx* sternohyoid muscle, typically thought to be associated with muscle damage and subsequent regeneration. Enhanced inflammatory cell infiltrate drives a fibrotic environment (Pelosi et al., 2015b). Indeed, we observed a significant increase in the collagen content of the *mdx* sternohyoid. Fibrosis is well characterised in the diaphragm of *mdx* mice (Stedman *et al.*, 1991), but to our knowledge this is the first report of enhanced collagen deposition in a complementary muscle of breathing, the sternohyoid. Enhanced collagen deposition within the muscle impairs muscle functional performance, which given the role of the sternohyoid as an airway dilator has implications for adequate control of airway calibre in DMD.

DMD patients and the *mdx* mouse have elevated levels of circulating pro-inflammatory cytokines, namely IL-1, IL-6 and TNFα (Gosselin & Williams, 2006), promoting an inflammatory response associated with dystrophic changes (Kumar & Boriek, 2003). Anti-inflammatory treatment with glucocorticoids is the main treatment strategy in delaying loss of ambulation in DMD but treatment is unfortunately associated with deleterious side effects (Pichavant *et al.*, 2011). Therefore, there is a need for new therapeutic strategies that can rescue or at least halt muscle impairments in DMD.

IL-6 is a pleiotropic cytokine, exhibiting both pro and anti-inflammatory properties, hence mediating diverse biological functions (Pedersen & Febbraio, 2008). Several studies have targeted pro-inflammatory cytokine signalling in *mdx* and examined their respective roles in the dystrophic process. TNF-α inhibition has been shown to have beneficial effects in *mdx* mice (Messina *et al.*, 2006; Messina *et al.*, 2009). IL-6 has been shown to promote muscle

atrophy in rats (Haddad *et al.*, 2005) and mice (Tsujinaka *et al.*, 1996), which is amenable to blockade. Additionally, *mdx* mice crossed with mice overexpressing IL-6, present with a significant reduction in limb muscle force and a decline in performance during treadmill exercise, indicative of impaired muscle function (Pelosi *et al.*, 2015b). Treatment with an xIL-6R antibody, blocking IL-6 signalling, has been shown to decrease pro-inflammatory cytokine expression in the diaphragm, improving treadmill performance in *mdx* mice (Pelosi et al., 2015b).

In the present study, co-administration of an IL-6 neutralising antibody (xIL-6R) and a CRFR2 agonist (Uro-2) in *mdx* mice resulted in significantly increased force-generating capacity compared with *mdx* mice treated with saline (~86% increase). Specific force in *mdx* sternohyoid following treatment was increased to values equivalent to WT saline. Drug treatment increased *mdx* sternohyoid work, power and shortening velocity over the load continuum (0-60% max tension). Increased work production following treatment in *mdx* is due to a positive inotropic effect on force-generating capacity since we observed no significant difference in peak shortening between *mdx* treatment and *mdx* saline. In contrast, increased *mdx* sternohyoid power production is due to both an increase in force-generating capacity and shortening velocity. Drug treatment in WT also had a positive inotropic effect on force generation (~49% increase) compared with WT saline. For WT, drug treatment increased sternohyoid work and power as a function of load bearing, both of which are due to an inotropic effect on muscle force. Significant increases in WT sternohyoid specific force suggest direct inotropic effects of drug co-treatment on sternohyoid muscle fibres. However, it should be noted that we determined tissue, and not fibre, CSA for our calculation of specific force. Therefore, whilst our measurement accounts for force normalised to tissue CSA, it does not account for alterations in myofibre CSA, which contribute to force-

generation in muscle. This is an important distinction since drug co-treatment caused fibre hypertrophy in WT (but not *mdx*) muscle. Uro-2 elevates cAMP, protein kinase A and the cAMP-binding protein Epac (Reutenauer-Patte et al., 2012), and improves calcium homeostasis in calcium over-loaded *mdx* striated muscle with beneficial protective effects reducing muscle necrosis (Reutenauer-Patte et al., 2012). CRFR2 agonists increase muscle fibre mass, with evidence of increased muscle fibre CSA and absolute muscle force (Hinkle et al. 2004), in addition to actions that prevent atrophying of muscle in various experimental models (Hinkle et al., 2003, 2004). As such, we posit that fibre hypertrophy likely contributed to enhanced force generation in WT sternohyoid. It remains unclear however, if drug co-treatment exerted direct inotropic effects on myofibres contributing to muscle force. Of interest, direct positive inotropic effects of Uro-2 have been noted in the treatment of heart failure (Bale et al, 2004) and Uro-2 has been shown to exert a positive inotropic effect in the isolated rat heart through cAMP-dependent mechanisms (Calderon-Sanchez et al., 2009), a major regulator of skeletal muscle contractility (Berdeaux et al., 2012).

Drug treatment in *mdx* mice significantly reduced type IIx and increased type IIb fibre distribution compared with untreated *mdx* saline. As such, drug treatment restored/ prevented fibre type transitions that are evident in the *mdx* saline group compared with WT saline. The preservation of type IIb fibres is likely contributing to the restoration of muscle force in *mdx* sternohyoid. Conversely, there was no difference in the distribution of any fibre type in the WT drug treatment group compared with WT saline. Uro-2 has been shown to induce anabolism in skeletal muscle (Reutenauer-Patte *et al.*, 2012). Anabolism in fibres supports increased force production, which could be beneficial to the dystrophic muscles of *mdx* mice. Interestingly, we observed hypertrophy of type IIb fibres in WT sternohyoid, but not *mdx*

sternohyoid following drug treatment, revealing a different structural basis for improved force comparing WT (hypertrophy) to *mdx* (fibre preservation).

Drug treatment in *mdx* slightly ameliorated sternohyoid muscle fibre central nucleation compared with *mdx* saline; conversely, percentage central nucleation was unaffected by treatment in WT sternohyoid. This suggests that drug treatment suppressed muscle fibre damage, resulting in fewer necrotic fibres, which should be beneficial for muscle performance. This observation highlights that muscle fibre preservation (and maturation to type IIb) is likely an important contributor to force generation in *mdx*-treated muscles in our study. However, of interest, drug treatment had no effect on collagen content or putative immune cell infiltration in *mdx* sternohyoid. As such, drug treatment was ineffective in reducing muscle fibrosis, perhaps resulting from muscle inflammation. As we did not characterise the nature of the infiltrate area (which we concede will also include non-immune cell types), we are unable to determine if drug treatment altered the cellular milieu in the interstitial spaces between myofibres. Chemokines were significantly increased in *mdx* sternohyoid muscle which is consistent with previous reports of elevated chemokines in muscle from *mdx* mice (Porter *et al.*, 2003; Demoule *et al.*, 2005). Interestingly, drug treatment in *mdx* significantly increased the content of chemo-attractant agents, suggesting that there may follow a heightened immune response in *mdx* muscle following drug treatment. Such a response could act to recruit immune cells to repair damaged muscle fibres, and thus lead to functional improvements in sternohyoid muscle, perhaps contributing to the impressive force recovery observed in our study.

From the present work we cannot ascertain which of the two drug treatments is responsible for the inotropic and structural effects observed in WT and *mdx* mice. Recent work

investigated the individual roles of xIL-6R and Uro-2 in improving *mdx* diaphragm force (Manning *et al.*, 2017). Of relevance to the current study, Manning et al. (2017) revealed an additive effect of xIL-6R and Uro-2 co-treatment on diaphragm muscle force providing the rationale for our combined drug approach. Additional studies describing the cellular mechanisms whereby xIL-6R and Uro-2 improve sternohyoid muscle function are warranted.

Our relatively short (2 week) intervention has yielded impressive findings, preserving sternohyoid muscle force-generating capacity in *mdx* mice. Although there are no temporal studies of the *mdx* sternohyoid during development to adulthood, the drug treatment began at a time when significant muscle remodelling is likely to be under way (based on work in *mdx* diaphragm (Coirault *et al.*, 2003). Intervention at a younger age and for a longer treatment duration would be an interesting study to explore the efficacy of the drug treatment before onset of muscle necrosis. It would also be of interest to determine if performance is preserved in older animals following treatment and if there are any adverse side effects due to prolonged drug treatment. Although drug treatment fully restored sternohyoid muscle force, there was no difference in the relative area of infiltration in the *mdx* sternohyoid drug-treatment group compared with *mdx* saline. Our data suggest that the beneficial effect of drug treatment on sternohyoid muscle fibre form and function is achieved without any apparent influence on local muscle inflammation and fibrosis, linked to on-going muscle fibre damage and repair. This suggests that the beneficial effect of the drug therapy relates to a retardation in muscle fibre damage allowing maturation of functional fibres, but without overt changes in muscle infiltrate. However, it is important to note that the nature of the inflammatory infiltrate may be favourably altered by drug treatment. Macrophages can exist in one of two states, M1 or M2. While M2 macrophages contribute to muscle repair, M1 macrophages can increase muscle fibre lysis (Villalta *et al.*, 2015). Therefore, depending on the state of the

infiltrating macrophage, inflammation can result in adaptive or maladaptive processes promoting regeneration or driving muscle wasting. We did not characterise the nature of the infiltrate in *mdx* muscle and therefore we cannot comment on the effect of drug treatment on the immune cell signature in *mdx* muscle. This requires further investigation, especially in the light of our observation that chemokines were increased in *mdx* and further increased by drug treatment, which may have established a beneficial immune response that favoured muscle performance. We also acknowledge that IL-6 blockade may have arrested beneficial actions of the myokine in muscle such as promoting myoblast proliferation and myotube formation.

In summary, *mdx* sternohyoid shows evidence of severe mechanical dysfunction and fibre type immaturity at an early age. Co-treatment with an anti-IL-6 receptor antibody and CRF-2 receptor agonist (Uro-2) had a positive inotropic effect, restoring mechanical force and power in dystrophic sternohyoid muscle. Drug treatment preserved fibre complement in *mdx* sternohyoid and slightly ameliorated the proportion of fibres with evidence of central nucleation indicative of damage. Preservation of MHC type IIb fibres as well as a partial reduction in centronucleation suggesting a preservation of functional fibres may underpin, at least in part, recovery of force production in the *mdx* drug-treated mice. Following a relatively short drug intervention period, recovery of contractile function was impressive in our study highlighting the potential utility of this combination therapy in DMD.

Acknowledgements

DPB was supported by funding from the Department of Physiology, UCC. The monoclonal anti-IL-6 receptor antibody was gifted by Chugai Pharmaceuticals, Tokyo, Japan. We are grateful to staff of the Biological Services Unit, UCC for support with animal care and welfare. We are grateful to Dr. G. Jasionek, Department of Physiology, UCC for technical support.

Disclosures

The authors have no financial, professional or personal conflicts relating to this publication.

Author contributions

DPB: experimental design; acquisition of data; analysis and interpretation of data; drafting of the original manuscript; JR: acquisition of data; analysis; LC: acquisition of data; analysis; KM: acquisition of data; analysis; MB: acquisition of data; analysis; DOM: experimental design; critical revision of the manuscript for important intellectual content; KOH: experimental design; interpretation of data; drafting and critical revision of the manuscript for important intellectual content; DE: experimental design; data acquisition; interpretation of data; drafting and critical revision of the manuscript for important intellectual content.

5. References

Attal P, Lambert F, Marchand-Adam S, Bobin S, Pourny JC, Chemla D, Lecarpentier Y & Coirault C (2000). Severe mechanical dysfunction in pharyngeal muscle from adult mdx mice. *Am J Respir Crit Care Med* **162,** 278-281.

Barbé F, Quera-Salva MA, McCann C, Gajdos P, Raphael JC, de Lattre J & Agustí AG (1994). Sleep-related respiratory disturbances in patients with Duchenne muscular dystrophy. *Eur Respir J* **7,** 1403-1408.

Bates G, Sigurdardottir S, Kachmar L, Zitouni NB, Benedetti A, Petrof BJ, Rassier D & Lauzon AM (2013). Molecular, cellular, and muscle strip mechanics of the mdx mouse diaphragm. *Am J Physiol Cell Physiol* **304,** C873-880.

Beck J, Weinberg J, Hamnegård CH, Spahija J, Olofson J, Grimby G & Sinderby C (2006). Diaphragmatic function in advanced Duchenne muscular dystrophy. *Neuromuscul Disord* **16,** 161-167.

Bersanini C, Khirani S, Ramirez A, Lofaso F, Aubertin G, Beydon N, Mayer M, Maincent K, Boulé M & Fauroux B (2012). Nocturnal hypoxaemia and hypercapnia in children with neuromuscular disorders. *Eur Respir J* **39,** 1206-1212.

Bulfield G, Siller WG, Wight PA & Moore KJ (1984). X chromosome-linked muscular dystrophy (mdx) in the mouse. *Proc Natl Acad Sci U S A* **81,** 1189-1192.

Burns DP, Edge D, O'Malley D & O'Halloran KD (2015). Respiratory Control in the mdx Mouse Model of Duchenne Muscular Dystrophy. *Adv Exp Med Biol* **860,** 239-244.

Burns DP & O'Halloran KD (2016). Evidence of hypoxic tolerance in weak upper airway muscle from young mdx mice. *Respir Physiol Neurobiol* **226,** 68-75.

Coirault C, Lambert F, Marchand-Adam S, Attal P, Chemla D & Lecarpentier Y (1999). Myosin molecular motor dysfunction in dystrophic mouse diaphragm. *Am J Physiol* **277,** C1170-1176.

Coirault C, Pignol B, Cooper RN, Butler-Browne G, Chabrier PE & Lecarpentier Y (2003). Severe muscle dysfunction precedes collagen tissue proliferation in mdx mouse diaphragm. *J Appl Physiol (1985)* **94,** 1744-1750.

De Bruin PF, Ueki J, Bush A, Khan Y, Watson A & Pride NB (1997). Diaphragm thickness and inspiratory strength in patients with Duchenne muscular dystrophy. *Thorax* **52,** 472-475.

Deconinck N & Dan B (2007). Pathophysiology of duchenne muscular dystrophy: current hypotheses. *Pediatr Neurol* **36,** 1-7.

Demoule A, Divangahi M, Danialou G, Gvozdic D, Larkin G, Bao W & Petrof BJ (2005). Expression and regulation of CC class chemokines in the dystrophic (mdx) diaphragm. *Am J Respir Cell Mol Biol* **33,** 178-185.

Emery AE (1991). Population frequencies of inherited neuromuscular diseases--a world survey. *Neuromuscul Disord* **1,** 19-29.

Evans NP, Misyak SA, Robertson JL, Bassaganya-Riera J & Grange RW (2009a). Dysregulated intracellular signaling and inflammatory gene expression during initial disease onset in Duchenne muscular dystrophy. *Am J Phys Med Rehabil* **88,** 502-522.

Evans NP, Misyak SA, Robertson JL, Bassaganya-Riera J & Grange RW (2009b). Immune-mediated mechanisms potentially regulate the disease time-course of duchenne muscular dystrophy and provide targets for therapeutic intervention. *PM R* **1,** 755-768.

Gosselin LE & Williams JE (2006). Pentoxifylline fails to attenuate fibrosis in dystrophic (mdx) diaphragm muscle. *Muscle Nerve* **33,** 820-823.

Haddad F, Zaldivar F, Cooper DM & Adams GR (2005). IL-6-induced skeletal muscle atrophy. *J Appl Physiol (1985)* **98,** 911-917.

Hall JE, Kaczor JJ, Hettinga BP, Isfort RJ & Tarnopolsky MA (2007). Effects of a CRF2R agonist and exercise on mdx and wildtype skeletal muscle. *Muscle Nerve* **36,** 336-341.

Hill NS, Redline S, Carskadon MA, Curran FJ & Millman RP (1992). Sleep-disordered breathing in patients with Duchenne muscular dystrophy using negative pressure ventilators. *Chest* **102,** 1656-1662.

Hinkle RT, Donnelly E, Cody DB, Bauer MB & Isfort RJ (2003). Urocortin II treatment reduces skeletal muscle mass and function loss during atrophy and increases nonatrophying skeletal muscle mass and function. *Endocrinology* **144,** 4939-4946.

Hukins CA & Hillman DR (2000). Daytime predictors of sleep hypoventilation in Duchenne muscular dystrophy. *Am J Respir Crit Care Med* **161,** 166-170.

Jonsdottir IH, Schjerling P, Ostrowski K, Asp S, Richter EA & Pedersen BK (2000). Muscle contractions induce interleukin-6 mRNA production in rat skeletal muscles. *J Physiol* **528 Pt 1,** 157-163.

Kumar A & Boriek AM (2003). Mechanical stress activates the nuclear factor-kappaB pathway in skeletal muscle fibers: a possible role in Duchenne muscular dystrophy. *FASEB J* **17,** 386-396.

Lewis P, Sheehan D, Soares R, Coelho AV & O'Halloran KD (2016). Redox Remodeling Is Pivotal in Murine Diaphragm Muscle Adaptation to Chronic Sustained Hypoxia. *Am J Respir Cell Mol Biol* **55,** 12-23.

Lewis P, Sheehan D, Soares R, Varela Coelho A & O'Halloran KD (2015). Chronic sustained hypoxia-induced redox remodeling causes contractile dysfunction in mouse sternohyoid muscle. *Front Physiol* **6,** 122.

Lynch GS, Hinkle RT, Chamberlain JS, Brooks SV & Faulkner JA (2001). Force and power output of fast and slow skeletal muscles from mdx mice 6-28 months old. *J Physiol* **535,** 591-600.

Manning J, Buckley MM, O'Halloran KD & O'Malley D (2016). In vivo neutralization of IL-6 receptors ameliorates gastrointestinal dysfunction in dystrophin-deficient mdx mice. *Neurogastroenterol Motil* **28,** 1016-1026.

Manning J, Buckley MM, O'Halloran KD & O'Malley D (2017). Combined xIL-6R and urocortin-2 treatment restores mdx diaphragm muscle force. *Muscle Nerve*.

Manning J & O'Malley D (2015). What has the mdx mouse model of duchenne muscular dystrophy contributed to our understanding of this disease? *J Muscle Res Cell Motil*.

Mantilla CB & Sieck GC (2003). Invited review: Mechanisms underlying motor unit plasticity in the respiratory system. *J Appl Physiol (1985)* **94,** 1230-1241.

Messina S, Bitto A, Aguennouz M, Mazzeo A, Migliorato A, Polito F, Irrera N, Altavilla D, Vita GL, Russo M, Naro A, De Pasquale MG, Rizzuto E, Musarò A, Squadrito F & Vita G (2009). Flavocoxid counteracts muscle necrosis and improves functional properties in mdx mice: a comparison study with methylprednisolone. *Exp Neurol* **220,** 349-358.

Messina S, Bitto A, Aguennouz M, Minutoli L, Monici MC, Altavilla D, Squadrito F & Vita G (2006). Nuclear factor kappa-B blockade reduces skeletal muscle degeneration and enhances muscle function in Mdx mice. *Exp Neurol* **198,** 234-241.

Messina S, Vita GL, Aguennouz M, Sframeli M, Romeo S, Rodolico C & Vita G (2011). Activation of NF-kappaB pathway in Duchenne muscular dystrophy: relation to age. *Acta Myol* **30,** 16-23.

Moran EM & Mastaglia FL (2014). Cytokines in immune-mediated inflammatory myopathies: cellular sources, multiple actions and therapeutic implications. *Clin Exp Immunol* **178,** 405-415.

Nowak KJ & Davies KE (2004). Duchenne muscular dystrophy and dystrophin: pathogenesis and opportunities for treatment. *EMBO Rep* **5,** 872-876.

O'Halloran KD (2006). Effects of nicotine on rat sternohyoid muscle contractile properties. *Respir Physiol Neurobiol* **150,** 200-210.

O'Halloran KD, McGuire M, O'Hare T & Bradford A (2002). Chronic intermittent asphyxia impairs rat upper airway muscle responses to acute hypoxia and asphyxia. *Chest* **122,** 269-275.

O'Leary AJ & O'Halloran KD (2016). Diaphragm muscle weakness and increased UCP-3 gene expression following acute hypoxic stress in the mouse. *Respir Physiol Neurobiol* **226,** 76-80.

Okazaki M, Yamada Y, Nishimoto N, Yoshizaki K & Mihara M (2002). Characterization of anti-mouse interleukin-6 receptor antibody. *Immunol Lett* **84,** 231-240.

Pastoret C & Sebille A (1995). Age-related differences in regeneration of dystrophic (mdx) and normal muscle in the mouse. *Muscle Nerve* **18,** 1147-1154.

Pedersen BK & Febbraio MA (2008). Muscle as an endocrine organ: focus on muscle-derived interleukin-6. *Physiol Rev* **88,** 1379-1406.

Pelosi L, Berardinelli MG, De Pasquale L, Nicoletti C, D'Amico A, Carvello F, Moneta GM, Catizone A, Bertini E, De Benedetti F & Musarò A (2015a). Functional and Morphological Improvement of Dystrophic Muscle by Interleukin 6 Receptor Blockade. *EBioMedicine* **2,** 285-293.

Pelosi L, Berardinelli MG, Forcina L, Spelta E, Rizzuto E, Nicoletti C, Camilli C, Testa E, Catizone A, De Benedetti F & Musarò A (2015b). Increased levels of interleukin-6 exacerbate the dystrophic phenotype in mdx mice. *Hum Mol Genet* **24,** 6041-6053.

Pichavant C, Aartsma-Rus A, Clemens PR, Davies KE, Dickson G, Takeda S, Wilton SD, Wolff JA, Wooddell CI, Xiao X & Tremblay JP (2011). Current status of pharmaceutical and genetic therapeutic approaches to treat DMD. *Mol Ther* **19,** 830-840.

Polla B, D'Antona G, Bottinelli R & Reggiani C (2004). Respiratory muscle fibres: specialisation and plasticity. *Thorax* **59,** 808-817.

Porter JD, Guo W, Merriam AP, Khanna S, Cheng G, Zhou X, Andrade FH, Richmonds C & Kaminski HJ (2003). Persistent over-expression of specific CC class chemokines correlates with macrophage and T-cell recruitment in mdx skeletal muscle. *Neuromuscul Disord* **13,** 223-235.

Reutenauer-Patte J, Boittin FX, Patthey-Vuadens O, Ruegg UT & Dorchies OM (2012). Urocortins improve dystrophic skeletal muscle structure and function through both PKA- and Epac-dependent pathways. *Am J Pathol* **180,** 749-762.

Rufo A, Del Fattore A, Capulli M, Carvello F, De Pasquale L, Ferrari S, Pierroz D, Morandi L, De Simone M, Rucci N, Bertini E, Bianchi ML, De Benedetti F & Teti A (2011). Mechanisms inducing low bone density in Duchenne muscular dystrophy in mice and humans. *J Bone Miner Res* **26,** 1891-1903.

Schiaffino S & Reggiani C (2011). Fiber types in mammalian skeletal muscles. *Physiol Rev* **91,** 1447-1531.

Smith PE, Edwards RH & Calverley PM (1989). Ventilation and breathing pattern during sleep in Duchenne muscular dystrophy. *Chest* **96,** 1346-1351.

Stedman HH, Sweeney HL, Shrager JB, Maguire HC, Panettieri RA, Petrof B, Narusawa M, Leferovich JM, Sladky JT & Kelly AM (1991). The mdx mouse diaphragm reproduces the degenerative changes of Duchenne muscular dystrophy. *Nature* **352,** 536-539.

Suresh S, Wales P, Dakin C, Harris MA & Cooper DG (2005). Sleep-related breathing disorder in Duchenne muscular dystrophy: disease spectrum in the paediatric population. *J Paediatr Child Health* **41,** 500-503.

Tsujinaka T, Fujita J, Ebisui C, Yano M, Kominami E, Suzuki K, Tanaka K, Katsume A, Ohsugi Y, Shiozaki H & Monden M (1996). Interleukin 6 receptor antibody inhibits muscle atrophy and modulates proteolytic systems in interleukin 6 transgenic mice. *J Clin Invest* **97,** 244-249.

Van de Graaff WB, Gottfried SB, Mitra J, van Lunteren E, Cherniack NS & Strohl KP (1984). Respiratory function of hyoid muscles and hyoid arch. *J Appl Physiol* **57,** 197-204.

Villalta SA, Rosenberg AS & Bluestone JA (2015). The immune system in Duchenne muscular dystrophy: Friend or foe. *Rare Dis* **3,** e1010966.

White DP & Younes MK (2012). Obstructive sleep apnea. *Compr Physiol* **2,** 2541-2594.

Whitham M & Febbraio MA (2016). The ever-expanding myokinome: discovery challenges and therapeutic implications. *Nat Rev Drug Discov*.

Williams R, Lemaire P, Lewis P, McDonald FB, Lucking E, Hogan S, Sheehan D, Healy V & O'Halloran KD (2015). Chronic intermittent hypoxia increases rat sternohyoid muscle NADPH oxidase expression with attendant modest oxidative stress. *Front Physiol* **6,** 15.

Figure Legends:

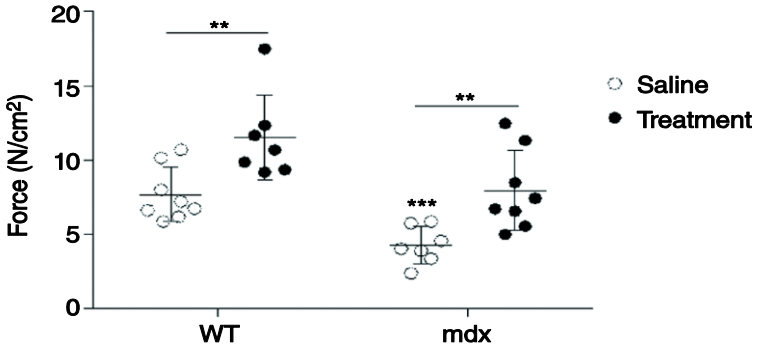

Figure 1. Peak Isometric Tetanic Force

Group data (mean ± S.D.) for tetanic force in WT (n=7-8) and *mdx* (n=7-8) sternohyoid muscle following 6 sub-cutaneous injections with saline (0.9% w/v) or treatment (xIL-6R (0.2 mg/kg) and Uro-2 (30 μg/kg); co-administered) over two weeks. Peak tetanic force was measured following stimulation at 100Hz *ex vivo*. Data were statistically compared by two-way ANOVA followed by Bonferroni post-hoc test.

** $P < 0.01$

Genotype: *** $P = 0.0003$; treatment $P = 0.0001$; interaction $P = 0.9$.

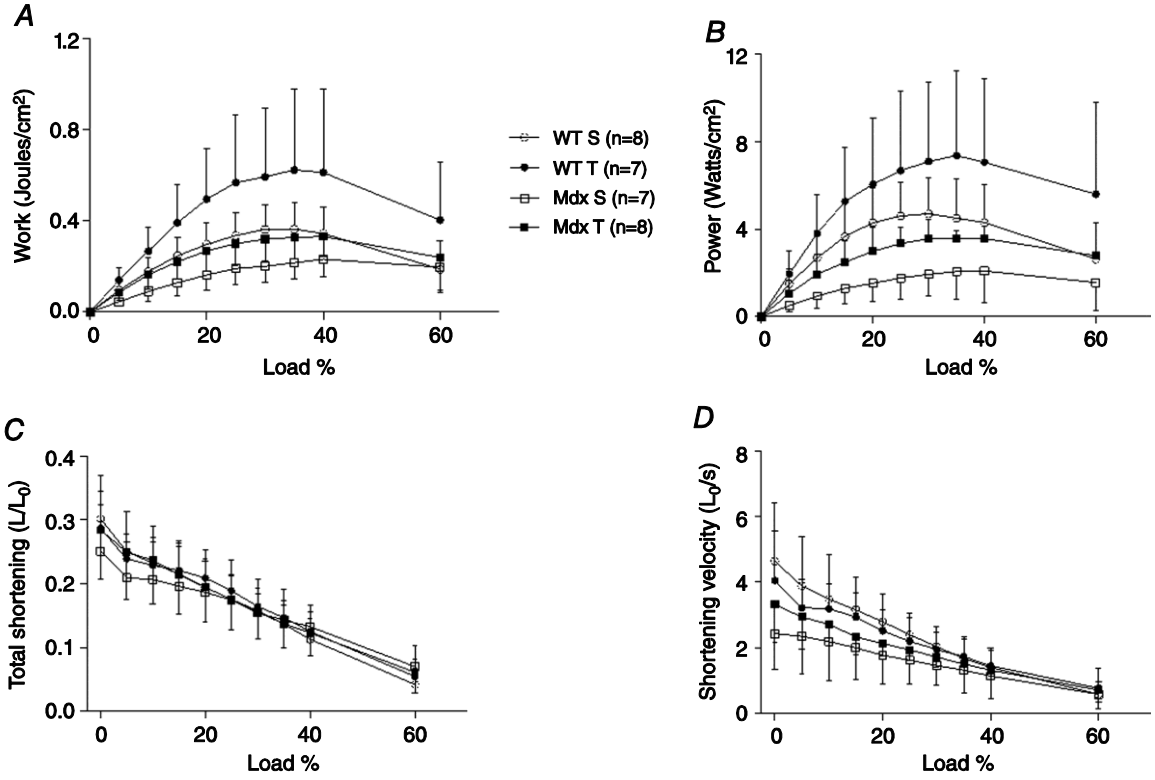

Figure 2. Sternohyoid Muscle Isotonic Contractile Properties

Group data (mean ± S.D.) for work-load (A), power-load (B), shortening-load (C) and shortening velocity-load (D) relationships in WT (n=7-8) and *mdx* (n=7-8) sternohyoid muscle following 6 subcutaneous injections of saline (0.9% w/v) or treatment (xIL-6R (0.2 mg/kg) and Uro-2 (30 µg/kg); co-administered) over two weeks. Data were statistically compared by two-way ANOVA.

Work: load $P < 0.0001$; genotype $P < 0.0001$; WT treatment $P < 0.0001$; *mdx* treatment $P < 0.0001$.
Power: load $P < 0.0001$; genotype $P < 0.0001$; WT treatment $P < 0.0001$; *mdx* treatment $P < 0.0001$.
Shortening: load $P < 0.0001$; genotype $P = 0.2$; WT treatment $P = 0.5$; *mdx* treatment $P = 0.2$.
Velocity: load $P < 0.0001$; genotype $P < 0.0001$; WT treatment $P = 0.2$; *mdx* treatment $P = 0.002$.

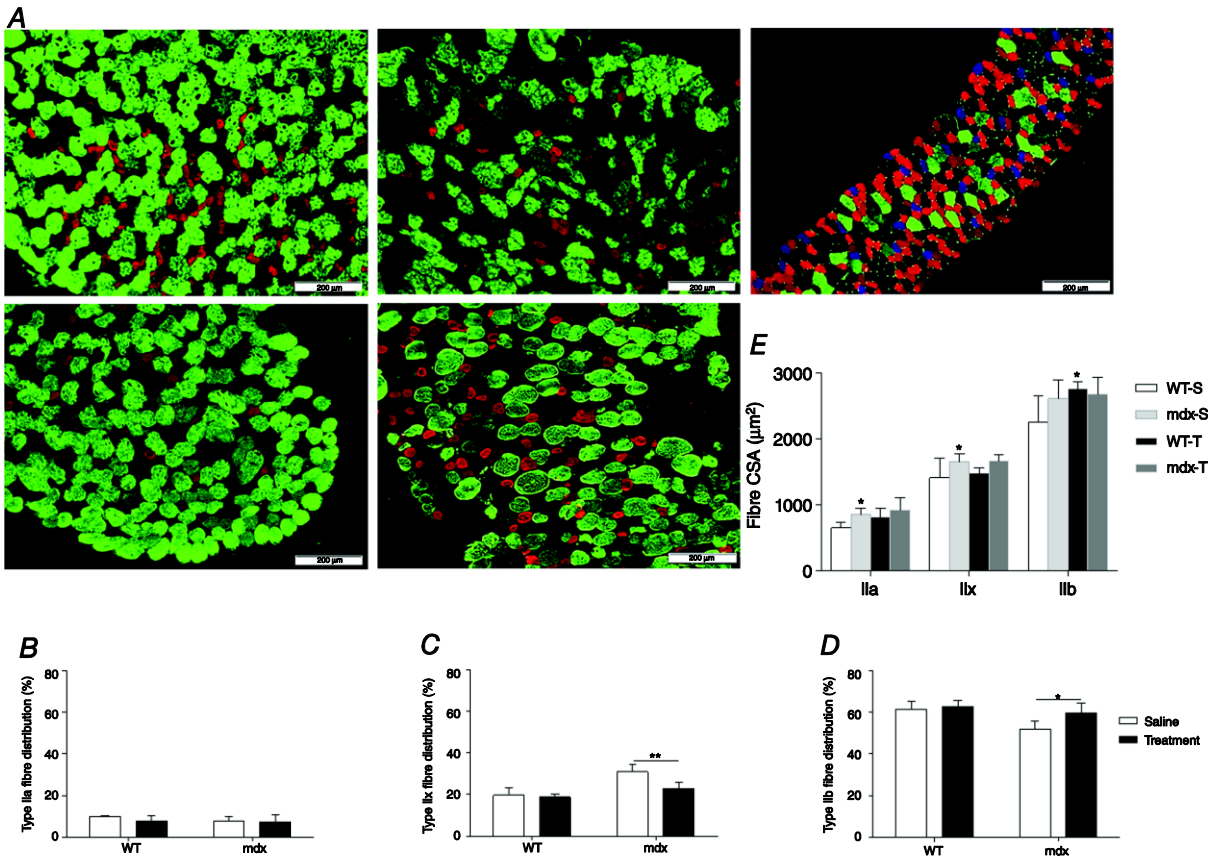

Figure 3. Sternohyoid Muscle Fibre Distribution and Cross Sectional Area

Representative immunofluorescence images of Sternohyoid (SH) muscle fibre type distribution (A), showing type IIa fibres (red), type IIx (untagged, appearing black) and type IIb (green) for WT saline (top left), *mdx* saline (top middle), WT drug-treated (bottom left) and *mdx* drug-treated (bottom middle). Note: the mouse sternohyoid muscle is devoid of type I – slow fibres, a positive control from type I fibre staining is shown in a section of WT mouse diaphragm (top right). Scale bars = 200 µm. Group data (mean ± S.D.) showing fibre distribution of type IIa fibres (B), type IIx (C) and type IIb (D) in WT (n=4) and *mdx* saline treated mice (n=5), and WT drug-treated (n=4) and *mdx* drug-treated mice (n=4). Mice received 6 sub-cutaneous injections of saline (0.9% w/v) or treatment (xIL-6R (0.2 mg/kg) and Uro-2 (30 µg/kg); co-administered) over two weeks. Data were statistically compared by two-way ANOVA followed by Bonferroni post-hoc test. In *mdx* mice, type IIx areal density was significantly increased (C), whereas type IIb fibre distrubution was decreased (D). With drug treatment, type IIx fibre distribution was significantly decreased in *mdx* mice compared with *mdx* saline (C), while type IIb fibre distribution (D) was increased compared with *mdx* saline.

* P < 0.05; ** *P* < 0.01.

B) Genotype *P* = 0.3; treatment *P* = 0.3; interaction *P* = 0.4.

C) Genotype *P* = 0.0001; treatment *P* = 0.007; interaction *P* = 0.03.

D) Genotype *P* = 0.006; treatment *P* = 0.04; interaction *P* = 0.1

Group data (mean ± S.D.) showing mean CSAs of sternohyoid muscle fibre type IIa, type IIx and type IIb (E). The CSA of type IIa and type IIx fibres was significantly increased in *mdx* mice. Drug treatment increased the CSA of type IIb fibres in WT mice only.

Type IIa: Genotype * *P* = 0.03; treatment *P* = 0.08; interaction *P* = 0.5.

Type IIx: Genotype * *P* = 0.02; treatment *P* = 0.6; interaction *P* =0.8.

Type IIb: Genotype *P* = 0.3; treatment: * *P* = 0.049; interaction *P* = 0.1.

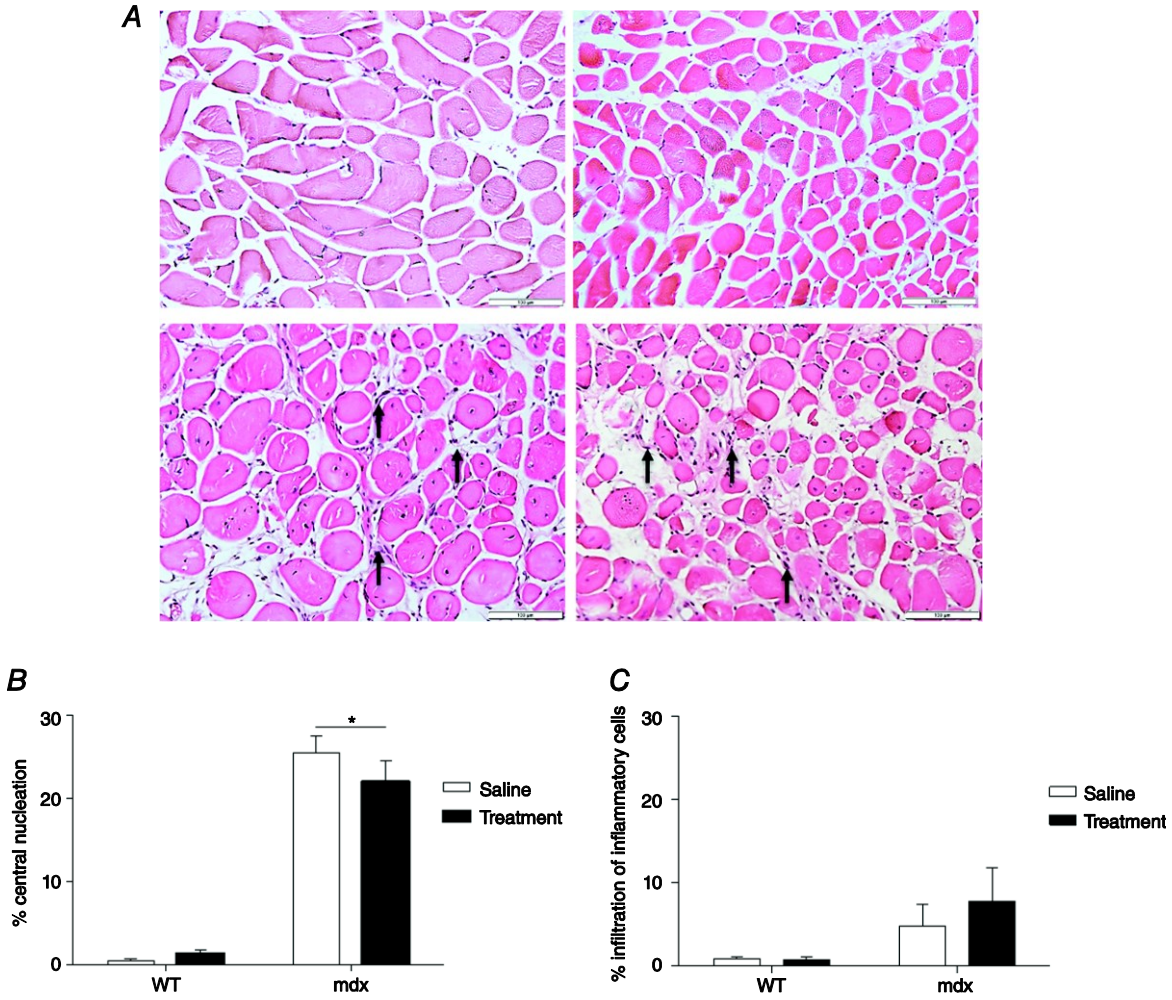

Figure 4. Central Nucleation and Inflammatory Cell Infiltration of Sternohyoid Muscle

Representative histological images (A) of sternohyoid muscle transverse sections stained with H&E in WT saline (top left), *mdx* saline (bottom left), WT drug-treated (top right) and *mdx* drug-treated (bottom right) scale bars 100 µm. Peripherally located nuclei are apparent in WT saline and WT drug-treated images. In comparison, *mdx* mice (saline and drug-treated) displayed an increased incidence of centrally located nuclei. Inflammatory cell infiltration is not apparent in WT saline and WT drug-treated groups. *Mdx* muscle (saline and treatment) displayed inflammatory cell infiltration, highlighted with black arrows.

Group data (mean ± S.D.) showing percentage of central nucleation (B) and percentage of infiltration of inflammatory cells (C) in sternohyoid muscle from saline-treated WT (n=4-5) and saline-treated *mdx* mice (n=5), and WT (n=4-5) and *mdx* (n=4-5) mice treated with xIL-6R (0.2 mg/kg) and Uro-2 (30 μg/kg) given as 6 sub-cutaneous injections over 2 weeks. Data were statistically compared by two-way ANOVA followed by Bonferroni post-hoc test. The percentage of centrally nucleated fibres was significantly increased in *mdx* mice. Drug treatment slightly ameliorated central nucleation in *mdx* mice only. The percentage of inflammatory cell infiltrates was significantly increased in *mdx* mice. Drug treatment did not affect this response; p=0.2284 compared with *mdx*. * p<0.05.

Central nucleation: Genotype $p < 0.0001$; treatment $p = 0.1$; interaction $p= 0.02$

Infiltration: Genotype: *** $p = 0.0002$, treatment $p = 0.2$; interaction $p = 0.2$

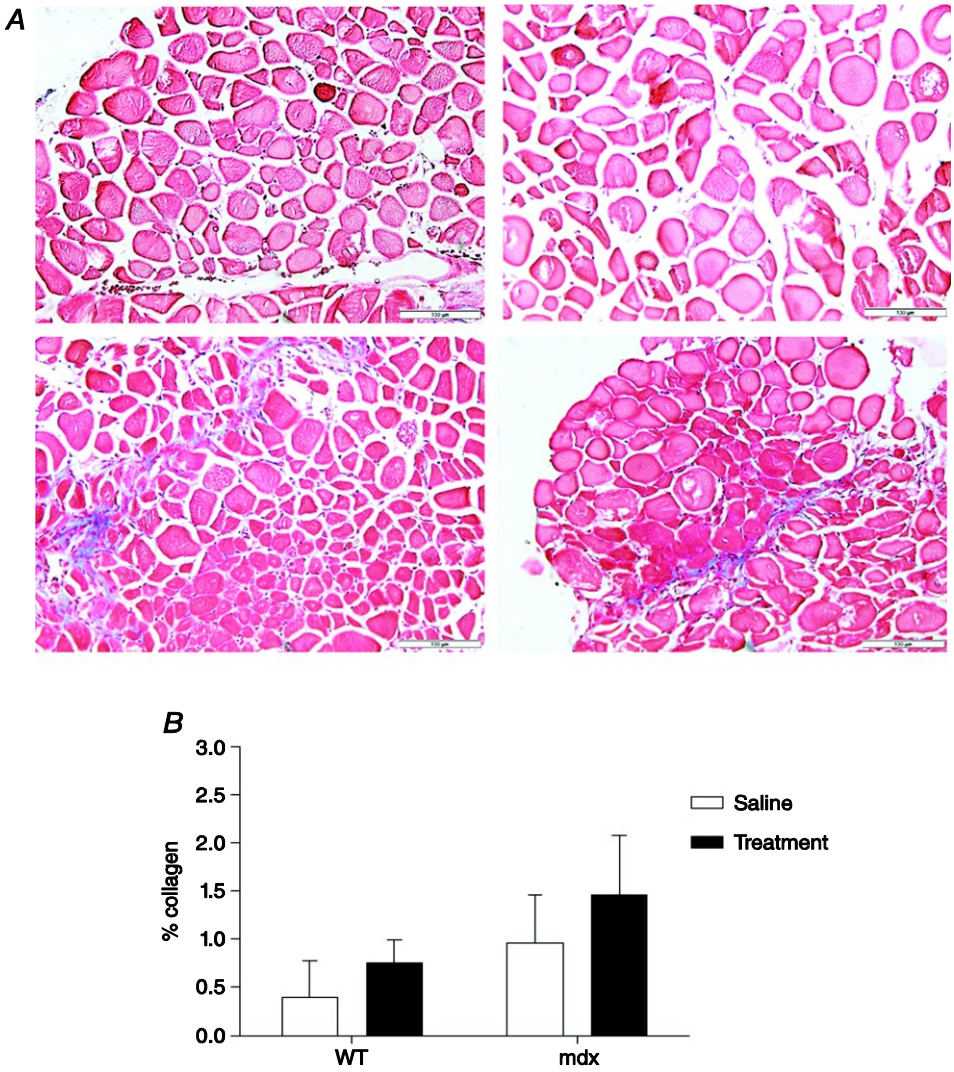

Figure 5. Collagen Deposition in Sternohyoid Muscle

Representative histological images (A) of sternohyoid muscle transverse sections stained with mason's trichrome in WT saline (top left), *mdx* saline (bottom left), WT drug-treated (top right) and *mdx* drug-treated (bottom right) scale bars 100 µm.

Group data (mean ± S.D.) showing percentage of collagen content (B) in sternohyoid muscle from saline-treated WT (n=5) and saline-treated *mdx* mice (n=4), and WT (n=4) and *mdx* (n=5) mice treated with xIL-6R (0.2 mg/kg) and Uro-2 (30 µg/kg) given as 6 sub-cutaneous injections over 2 weeks. Data were statistically compared by two-way ANOVA followed by Bonferroni post-hoc test. The percentage of collagen content was significantly increased in *mdx* mice. Drug treatment had no significant effect on collagen content for both WT and *mdx*.

Genotype: p = 0.0103, treatment: p = 0.0673; interaction p = 0.7779

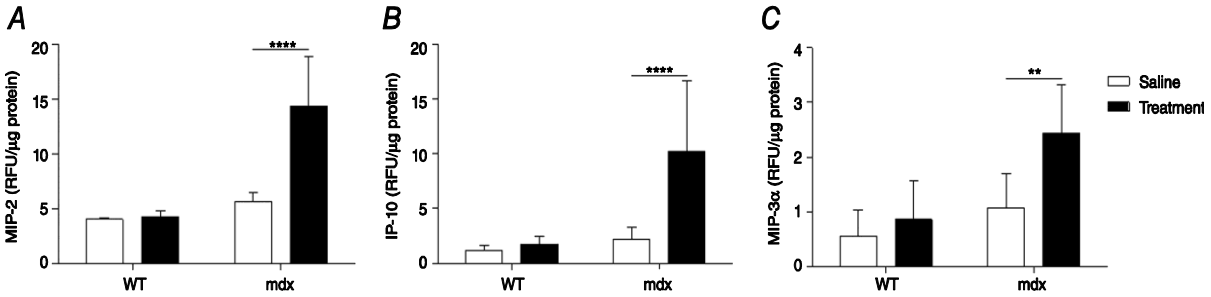

Figure 6. Chemokine Expression in Sternohyoid Muscle

Values (mean ± S.D.) for macrophage inflammatory protein 2 (MIP-2; A), interferon-γ induced protein (IP-10; B) and macrophage inflammatory protein-3 (MIP-3α; C) chemokine expression in sternohyoid muscle from WT (n=7-8) and *mdx* (n=7-8) mice injected sub-cutaneously with saline (0.9% w/v) or drug treatment (xIL-6R (0.2mg/kg) and Uro-2 (30µg/kg); co-administered) for two weeks. Data were statistically compared by two-way ANOVA followed by Bonferroni post-hoc test. ** $p < 0.01$; **** $p < 0.0001$

MIP-2: genotype: $p < 0.0001$; treatment $p < 0.0001$; interaction: $p < 0.0001$
IP-10: genotype: $p = 0.0002$; treatment: $p = 0.0007$; interaction: $p = 0.0022$
MIP-3α: genotype: $p = 0.0004$; treatment: $p = 0.0033$; interaction: $p = 0.0510$

	WT		*mdx*		Two-way ANOVA		
	Saline (n=8)	Treatment (n=7)	Saline (n=7)	Treatment (n=8)	Genotype	Treatment	Interaction
CT (ms)	11.7 ± 2.0	12.6 ± 3.4	17.0 ± 8.8	13.9 ± 4.3	*P* = 0.1	*P* = 0.6	*P* = 0.3
½ RT (ms)	18.2 ± 6.4	18.0 ± 5.8	23.4 ± 0.8	18.8 ± 5.7	*P* = 0.1	*P* = 0.2	*P* = 0.3
Twitch Force (N/cm^2)	1.2 ± 0.4	1.8 ± 0.6	0.5 ± 0.3 £	1.5 ± 0.8 #	*P* = 0.01	*P* = 0.0004	*P* = 0.5
Wmax (J/cm^2)	0.4 ± 0.1	0.6 ± 0.4 $	0.2 ± 0.08	0.3 ± 0.09	*P* = 0.004	*P* = 0.01	*P* = 0.2
Pmax (W/cm^2)	4.7 ± 1.7	7.4 ± 3.9	2.1 ± 1.5 £	3.6 ± 0.6	*P* = 0.0003	*P* = 0.01	*P* = 0.5
Smax (L/L_o)	0.3 ± 0.07	0.3 ± 0.06	0.3 ± 0.07	0.3 ± 0.08	*P* = 0.3	*P* = 0.7	*P* = 0.3
Vmax (L_o/s)	4.6 ± 1.8	4.1 ± 1.5	2.4 ± 1.1 £	3.3 ± 1.2	*P* = 0.008	*P* = 0.8	*P* = 0.2

Table 1. Sternohyoid muscle contractile properties.

Values (mean ± S.D.) for twitch contraction time (CT), twitch half-relaxation time (½ RT), peak twitch force, maximum mechanical work (Wmax), maximum mechanical power (Pmax), peak shortening (Smax) and peak shortening velocity (Vmax) of sternohyoid muscle from WT (n=7-8) and *mdx* (n=7-8) mice injected sub-cutaneously with saline (0.9% w/v) or drug treatment (xIL-6R (0.2mg/kg) and Uro-2 (30µg/kg); co-administered) for two weeks. Data were statistically compared by two-way ANOVA followed by Bonferroni post-hoc test.

£ *mdx* saline significantly different from corresponding WT saline value; $p < 0.05$

$ WT treatment significantly different from corresponding WT saline value, $p < 0.05$

mdx treatment significantly different from corresponding *mdx* saline value, $p < 0.05$